Enhancement of storage capacity of CO_2 in megaporous saline aquifers using nanoparticle-stabilized CO_2 foam

Feng Guo[a], Saman A. Aryana*[a], Yuhang Wang[b], J. Fred McLaughlin[c] and Kipp Coddington[c]

Abstract

Carbon dioxide sequestration in saline aquifers is a promising approach to reduce anthropogenic CO_2 emissions and mitigate global climate change. CO_2 storage capacity in aquifers depends on various factors such as interfacial tension, injection rate, viscosity ratio and characteristics of the porous media. We investigate the effects of these variables on CO_2 gas and foam injection into a brine-saturated porous medium using a glass fabricated microfluidic device. The pore network is a representation of Washita-Fredericksburg formation located at a depth of 1,110 m that is part of a saline aquifer located in southeast US and is currently under investigation to estimate its storage capacity as a commercial-scale CO_2 storage hub. Contact angles and interfacial tensions between different fluids are measured under the experimental conditions. The three different injection rates are studied for each gaseous and foam injection. The displacement patterns images are captured by a high-resolution camera with an achromatic 60MP sensor, and displacement performances are analyzed. CO_2 foam injection appears to significantly increase CO_2 storage in the microfluidic device (20%-40% higher compared to gas injection). Thus, CO_2 foam injection is a promising approach to reduce CO_2 mobility and enhance storage capacity in the target formation.

Keywords

CO_2 storage; Saline aquifer; Nanoparticles; Foam

Introduction

There is an overwhelming consensus amongst climatology scientists that global climate change is having significant and observable effects on the environment and is contributing to a number of catastrophic events such as rising surface temperature, rising sea level, and ocean acidification (NASA, 2018). The compounding effects of these problems poses significant risks to human life by affecting infrastructure and interconnected economic sectors, as reported by the Fourth National Climate Assessment (USGCRP, 2018). Anthropogenic CO_2 emissions make up approximately 80% of the total U.S. greenhouse gas emission and is the most significant greenhouse gas in terms of overall contribution to climate change.(IPCC, 2015) One promising approach to mitigate global climate change is long-term storage of anthropogenic CO_2 from point sources such as coal-fired power plants, cement plants, iron and steel plants (Leung et al., 2014). Geological CO_2 sequestration in saline aquifers, depleted oil and gas reservoirs, and coalbeds, is a potentially effective and practical approach to store CO_2 (Rahman, 2018; Yang et al., 2017). Deep saline aquifers constitute an attractive subset of subsurface targets for CO_2 storage due to their relatively large storage capacity and their relatively low probability of leakage of the stored CO_2. For example, the aquifer in the Statoil's Sleipner field provides approximately 1 million tons (Mt) of CO_2 storage per year and the site has not experienced any leakage since 1996 (Michael et al., 2010).

In such a geological CO_2 sequestration process, CO_2 is injected into the saline aquifer to displace the in-situ wetting phase brine. The injected CO_2 is stored in the aquifer through various trapping mechanisms, namely structural trapping, residue trapping, solubility trapping and mineral

[a] Department of Chemical Engineering, University of Wyoming, Laramie, USA. E-mail: saryana@uwyo.edu
[b] Department of Petroleum Engineering, University of Wyoming, Laramie, USA.
[c] Center for Economic Geology Research, University of Wyoming, Laramie, USA.

trapping. These mechanisms operate at different time-scales and contribute to the long-term stability of the storage process (Gershenzon et al., 2017; Rathnaweera et al., 2015; Zhao et al., 2014). Structural and residual trapping are considered as the most immediate and significant mode of trapping, and account for up to 95% of the storage resource (Al-Menhali and Krevor, 2016; Bachu, 2015; Dejam and Hassanzadeh, 2018; Krevor et al., 2015). During the displacement process, some of the resident brine, often referred to as residual brine, does not mobilize and remains in place. This phenomenon occurs during the drainage process and is mainly due to the relatively large contrasts of density and viscosity between CO_2 and the resident brine (Aryana and Kovscek, 2012; Pini and Krevor, 2019). These effects are magnified in megaporous reservoirs and dominate flow behaviour; hence, they hinder the CO_2 trapping process and may limit CO_2 flow through the aquifer's pore spaces (Li et al., 2017). Accordingly, reducing the mobility of CO_2 is an important challenge, which would mitigate the aforementioned viscosity and density contrasts and would ultimately enhance storage capacity by reducing the residual brine (Adebayo et al., 2017; Amirian et al., 2018). Gas-mobility control methods such as CO_2 foam injection, water-alternating-gas (WAG) injection and surfactant-alternating-gas (SAG) injection are possible approaches to control the mobility of CO_2 (Cui and Bourrel, 2018; Kamal et al., 2018; Siddiqui and Gajbhiye, 2017) Vitoonkijvanich et al. (Vitoonkijvanich et al., 2015) investigated the effects of CO_2 foam on the efficiency of CO_2 sequestration in a North Sea aquifer by co-injecting CO_2 and surfactants. Their results suggest that foam-assisted sequestration may significantly improve the storage efficiency at the cost of a marginal increase in water consumption compared with SAG. Siddiqui et al.(Siddiqui and Gajbhiye, 2017) improved storage efficiency of CO_2 in a sandstone core by foam flooding using co-injection with fluorosurfactant FS-51 and alpha-olefin-sulfonate (AOS) surfactants. Thus, CO_2 foam injection may be a promising solution to improve displacement efficiency and enhance CO_2 storage capacity in geologic formations.

Leakage of CO_2 and foaming additives to the surface or water-bearing formations is a substantial risk associated with CO_2 foam storage in saline aquifers (Barnes et al., 2016; Singh and Islam, 2018). Nanoparticle (NP)-assisted CO_2 foams are introduced to improve long-term CO_2 sequestration efficiency in aquifers, as well as, to prevent leakage of CO_2 and additives. NP-assisted CO_2 foam in EOR seems effective in improving sweep efficiency and oil recovery (Ehtesabi et al., 2014; Hendraningrat and Torsæter, 2015a; Hendraningrat and Torsæter, 2015b; Xu et al., 2015). Experimental studies suggest that compared to its individual constituents, namely CO_2 and water, foam improves oil recovery due to its significantly higher apparent viscosity and reduced mobility in both homogeneous and heterogeneous porous media (Guo and Aryana, 2016; Guo and Aryana, 2018; Guo et al., 2017). Potential storage gains, due to the use of NPs in CO_2 sequestration, are thus far only investigated in a handful of studies (Aminzadeh et al., 2013; Clark and Santiso, 2018; Yang et al., 2014). Moreover, most of the previous work is concerned with the use of core-flooding systems as a platform to investigate CO_2 sequestration efficiency and long-term CO_2 storage in saline aquifers (Hosseini et al., 2018; Rognmo et al., 2017).

On the other hand, a microfluidic platform coupled with high-resolution imaging offers important advantages in real-time and direct visualization and quantification of fluid interactions in porous media and the underlying trapping mechanisms relevant to CO_2 storage, and in the absence of complicating interactions such as geochemistry (Fu, 2016; Zheng et al., 2017). This work explores the efficacy of NP-stabilized CO_2 foam in improving displacement efficiency and storage capacity

of a porous medium using a glass microfluidic device in which the pore network is a representation of the Washita-Fredericksburg formation in east-central Mississippi.

1.1. Legislative Issues

Carbon capture storage (CCS) technology – including utilization of CO_2 for enhanced oil recovery and storage in deep saline and related geologic structures – is widely recognized as necessary for major fossil fuel facilities, including both coal and natural gas, to comply with current and future international, national and state-law climate requirements (IPCC, 2018). Internationally, both the current Kyoto Protocol and Paris Agreement, which will replace it in 2020, are anticipated to make use of CCS. Under the Kyoto Protocol, for example, the Clean Development Mechanism specifically envisioned the use of the technology. Its status under the Paris Agreement remains somewhat uncertain, and will not likely be resolved until late 2019 at the COP25 meetings (Dixon et al., 2013). Major international organizations such as the International Energy Agency and Intergovernmental Panel on Climate Change have issued favorable reports about the technology and the need for it (IEA, 2019).

Domestically in the United States at the federal level, the U.S. Environmental Protection similarly has built CCS technology into a variety of Clean Air Act regulatory programs (EPA, 2011). As of early 2019, several of these programs were in the midst of revision by the current U.S. policy (EPA, 2018b). The federal government's favorable view of the technology is unlikely to change. The U.S. Congress, for example, continues to appropriate monies to the U.S. Department of Energy to advance the technology (Office of Fossil Energy, 2019). And early in 2018, Congress based amendments to the section 45Q CCS tax credit to greatly expand it (45Q, 2018). Later in 2019, the Internal Revenue Service is expected to issue guidance under the credit.

States like California, for example, have also endorsed CCS. In early 2019, the California Air Resources Board finalized a CCS methodology that will allow the use of the technology under that State's Low Carbon Fuel Standard (California Air Resources Board, 2018).

1.2. Geological Context

The largest distribution of point-sources of anthropogenic CO_2 are located within the southeastern United States (EPA, 2018a). This has prompted support for regional geologic carbon storage research. Project ECO2S, funded by the US Department of Energy (FE-0029465) under its CarbonSAFE initiative, is one of the largest regional southeastern US carbon storage projects. It was established to determine the feasibility of developing a regional, commercial-scale CO_2 storage hub to investigate storage feasibility at the Project ECO2S study site in east-central Mississippi. Three stratigraphic test wells were drilled through three potential saline storage reservoirs; the Upper Cretaceous Tuscaloosa Group, the Lower Cretaceous Washita-Fredericksburg and the Paluxy formations (D. Riestenberg, 2018). These formations are located between depths of 1,110 to 1,750 m below the surface, which are suitable depths for supercritical CO_2 injection. All three formations are characterized by interbedded sandstone and mudstone. Petrophysical analysis from the three wells indicate targeted reservoir intervals are extremely porous given their age and depths (geometric mean of reservoir intervals averages between 26-29%) (D. Riestenberg, 2018). For this study, a reservoir interval was sampled from the Washita-Fredericksburg formation from well MPC 34-1. The sampled reservoir interval is ~3.5 m thick and consists of clean, cross-bedded sandstone (Fig.1).

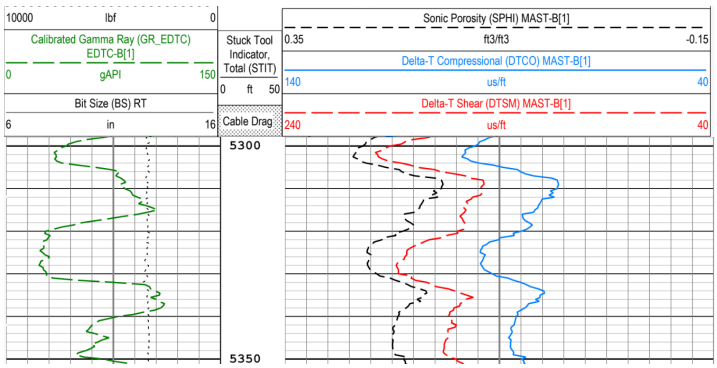

Fig. 1. Petrophysical log data from a Schlumberger Sonic Scanner log over the sampled reservoir interval (1619.1 to 1625.4 m, well MPC 34-1). Porosity estimates from the sonic log approaches 30% within the 3.7 m sand interval

2. Method and material

This part describes the fluids, microfluidic device and experimental procedures used in this work.

2.1. Fluids

The amorphous fumed silica T30 (unmodified, 100% SiOH coverage) was received in powder form and were gifts from Wacker-Chemie. NP dispersions were diluted to desired concentrations with deionized (DI) water (Nanopure II, Barnstead, Dubuque) and mixed with surfactant mixture alpha-Olefin Sulfonate (AOS) + Lauramidopropyl Betaine (LAPB) (Table 1). The brine solution is prepared by dissolving, in DI water, sodium chloride (Sigma Aldrich) and calcium chloride (Sigma Aldrich) with a wt% ratio of 4.4/1 and a total concentration of 85271 ppm, based on the salinity data from the Washita-Fredericksburg formation sampled via well MPC 34-1. The viscosity of brine was measured at 2.12cP using a spindle viscometer (DV2T, Brookfield) at a shear rate of 195.7 s^{-1} and a temperature of 20 °C. CO_2 (research grade, United States Welding, USA) and the surfactants were used as received without further treatment. Solution mixtures including isopropanol/ethanol/water (1:1:1), 2 M HCl solution, a base solution (DI water/NH_4OH/H_2O_2 at 5:1:1) and DI water were used to clean organic residue in the porous medium and syringe. Each fluid was degassed (Ultrasonic bath, Fisher Scientific) for 10 mins and filtered by a syringe filter (0.2 µm, Sterlitech) prior to injection in microfluidic device.

Table 1. Surfactants used to generate CO_2 foam with NPs

Type	Family	Name	Source
Anionic Surfactant	Alpha-Olefin Sulfonate	AOS 14-18 (AOS) 39% active	Stepan Co
Zwitterionic Surfactants	Betaine	LAPB 35% active	Rhodia Co

2.2. Microfluidic device

The mask of the porous medium used in fabrication of the microfluidic device was developed based on a mosaic of Scanning Electron Microscopy (SEM) images of a thin section of the Washita-Fredericksburg formation. Pore spaces were connected based throat size distribution data obtained from a mercury intrusion experiment. The resulting complex network of channels was representative of the geometries and connections of the three-dimensional sample of the formation.

Pore spaces in actual rock samples are connected in the three-dimensional space. These connections were reflected in the resulting two-dimensional map, and as such, the overall porosity of the map exceeded log estimates of porosity shown in Fig. 1. The map of the medium was then etched onto a borosilicate substrate using a photo lithography technique (Stjernström and Roeraade, 1998). The etched substrate was thermally bonded to a blank wafer to create the microfluidic device (Fig. 2). The total chip dimension was 2 inches x 2 inches with a pore network region of 36.39 mm x 26.39 mm and a porosity of approximately 45%. The average depth of the etched pore network was measured at approximately 10 μm, and the permeability of the microfluidic device was measured at approximately 15 mD.

The glass microfluidic device enabled visual observation of fluid flow under high-pressure condition without using a pressure cell. Unlike PDMS microfluidic devices the pore structure of the glass chip does not change during fluid flow under a pressure and parameters such as flow rate, fluid properties, and contact angle may be investigated reliably.

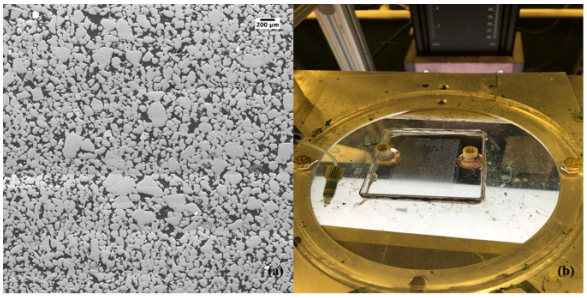

Fig. 2. SEM images of the thin-section (a) and the microfluidic device (b). Trapping is further challenged in megaporous reservoirs where buoyancy and structural trapping may dominate.

2.3. Injection Experiments

All displacement experiments were performed in the same microfluidic device. The microfluidic device was saturated with brine solution by injecting 40 pore-volumes (PV) of dyed brine (black) using a syringe pump (PHD Ultra, Harvard Apparatus). The outlet of microfluidic device was connected to a Parr vessel, which collected the brine drained from the microfluidic device. An ISCO pump (500D, Teledyne ISCO) was connected to the Parr vessel to maintain a constant backpressure of 300 psi. Even though our injection experiments were not conducted using pressures encountered in deep saline aquifers, the displacement of brine by gaseous CO_2 behaves in a highly unstable manner similar to that of supercritical CO_2 and may be considered as a reasonable proxy for the supercritical case.(Zheng et al., 2017) After each experiment, the microfluidic device was thoroughly cleaned using a cleaning protocol in the following order: DI water, isopropanol/ethanol/water (1:1:1), 2 M HCl solution, DI water, a basic solution (DI water/NH_4OH/H_2O_2 at 5:1:1) and DI water.

2.3.1. Gas injection

CO_2 was injected through one side of microfluidic device using an ISCO pump (100D, Teledyne ISCO) at a various volumetric flowrate (q). Three injection rates were used 0.1 μL/min, 1 μL/min and 10 μL/min which correspond Darcy velocities, 0.88 m/day, 8.8 and 88 m/day. Prior to the injection, the entire experimental system was purged with CO_2 to remove all air from the system.

At each flowrate, CO_2 was injected to displace dyed brine until CO_2 saturation appeared to have reached its ultimate value.

2.3.2. Foam injection

Foam was generated by injecting the NP-surfactant solution and gaseous CO_2 at P = 300 psi simultaneously into a stainless-steel tube filled with glass beads using two ISCO (pumps A and B shown in Fig. 2). The glass beads ranged in diameter from 105 µm to 210 µm. Glass beads were washed with H_2SO_4/H_2O_2 (4:1) and $NH_4OH/H_2O_2/H_2O$ (1:1:5) mixtures at their boiling points. The inner diameter of the stainless-steel tube is 15 mm, and the length is 50 mm. Glass fibers were used at both ends of the steel tube to hold the glass beads in place, and the outlet of the steel tube was connected to an inline filter (7µm, Swagelok).

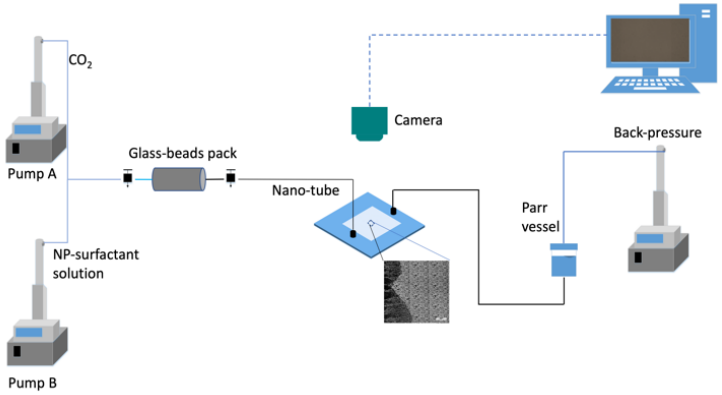

Fig. 3. Injection experiment set-up.

2.4. Data capture and processing

High-resolution images of the porous medium were captured during flow experiments using a monochromatic 60 MP sensor. Pixel intensities were used to analyze flow behavior and recovery rates, in other words the storage rate, in the porous medium. Recovery rates were calculated using captured images via three main steps (Wang and Aryana, 2019): i) perspective transformation (Szeliski, 2010); ii) exclusion of the grains, and iii) local thresholding. Perspective transformation was performed on each image to extract the portion that corresponded to the porous medium, and to correct minor misalignments. The transformation matrix was determined using coordinates of four points on both the original images and their corresponding target positions. Inspection of images revealed a slight non-uniformity in illumination across the porous medium. Therefore, instead of a global threshold value, a local thresholding strategy was used across the medium to delineate the two phases (Pal and Pal, 1993). Each image was partitioned into a set of sub-regions over which illumination was relatively uniform. The kernel density estimation method (Läuter, 1988), was used to build the histogram for each sub-region, and the corresponding threshold was determined based on Otsu's method (Otsu, 1979).

3. Results and discussion

Dimensionless capillary numbers (Ca) and viscosity ratios (M) are calculated for the injection experiments. Flow dynamics are determined by the interplay between capillary and viscous forces, whose relative magnitudes are quantified via these dimensionless numbers (Lenormand et al.,

1983). The capillary number is defined as $Ca = v\mu_1/\gamma$, where v is Darcy velocity of invading fluids, $\mu_1$is its viscosity and γ is the interfacial tension. M is defined as the ratio of the invading fluid viscosity, μ_1, to that of the displaced fluid, μ_2; $M = \mu_1/\mu_2$. Depending on these two parameters, either capillary or viscous forces dominate, leading to three basic displacement regimes: (1) viscous fingering, (2) capillary fingering or (3) stable displacement (Lenormand and Touboul, 1988). Based on their Ca and M numbers, the experiments are plotted on a logCa-logM diagram, where boundaries for the three displacement regimes are shown are reported in literature (Fig. 4). The three gas injection experiments, shown in black circles, are either in the capillary fingering regime or in the transition regime between viscous and capillary fingering. Foam injection experiments, shown in blue diamonds, are in the transition zone between capillary fingering and stable displacement. The viscosity of pure CO_2 gas is significantly lower than the viscosity of brine; this unfavorable viscosity contrast promotes the unstable flow patterns seen in displacement experiments. NP-stabilized CO_2 foams mitigate the viscosity contrast between invading fluids (foam) and residence fluids (brine), and thereby, reduce viscous fingering effects and improve CO_2 storage capacity in saline aquifers. Thus, the study of simultaneous flow of multiple phases in a porous medium provides valuable insights into geological carbon sequestration in saline aquifers (Carroll et al., 2015; Zhang et al., 2011). Moreover, interactions between the mineral surfaces, fluids, and CO_2 (interfacial tension and wettability) also have a significant impact on CO_2 sequestration and storage in deep saline aquifers (Kaveh et al., 2011).

3.1. Interfacial tension (IFT) and Contact angle

A high pressure and high temperature pendent drop interfacial tension cell (FDS CORP.) was used for the measurement of contact angle and IFT. In this study, every experiment was repeated at least 3 times. The IFT and contact angles were measured at the same pressure and temperature conditions as the flow experiments, i.e., 300 psi and 20 ^oC. Fig. 5 shows CO_2 droplets (black) on a Borofloat glass substrate at 300 psi and at atmospheric pressure. The average contact angle of CO_2 in the brine solution was measured at 67.8^o and 64.5^o, at 300 psi and at atmospheric pressure, respectively. Similarly, the average contact angle of CO_2 in the Si-LAPB+AOS solution was measured at 28.5^o and 21.7^o, at 300 psi and at atmospheric pressure, respectively. Dependence of contact angles on droplet generation and pressure may lead to a wettability change in aquifers during CO_2 sequestration. This effect may influence CO_2 storage capacity significantly (Al-Khdheeawi et al., 2017). The average measured IFT values between CO_2-brine solution, and CO_2-Si-LAPB+AOS solution pairs under 300 psi were measured at 32.28 mN/m and 11.26 mN/m, respectively. Values of IFT and contact angles affect capillary forces directly, which dominate two primary trapping mechanisms for CO_2 storage, namely structural trapping and residual trapping (Iglauer, 2017). This interaction is evident in the observed impact of pressure-dependent IFT and contact angles on fluid distribution and displacement behavior in porous media (Chalbaud et al., 2010). They strongly influence CO_2 injectivity, storage capacity and security (Espinoza and Santamarina, 2010). Microfluidic displacement experiments in porous media show a notable increase in CO_2 injectivity and a significant reduction in CO_2 mobility due to a lowered IFT resulting from the use of Si-LAPB+AOS mixtures (Guo and Aryana, 2016), which will, in turn, contribute to potentially significant increases in CO_2 storage capacity in subsurface settings.

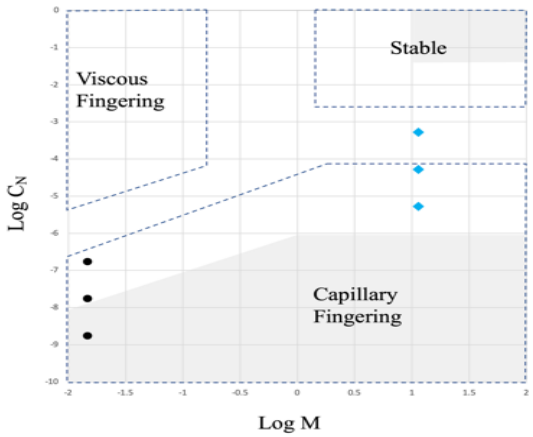

Fig. 4. Drainage flow regime diagram. Black dots represent experiments where CO_2 is used as the injectant; the blue dots represent experiments where CO_2 foam is used as the injectant. The shaded areas are based on work by Zhang et al. (Zhang et al., 2011) and the regimes delineated with dashed lines are based on work by Lenormand et al. (Lenormand et al., 1988)

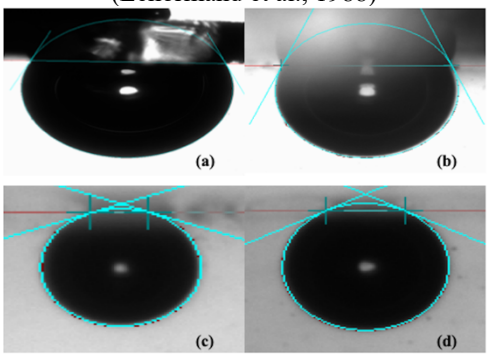

Fig. 5. Image of CO_2 droplets in MPC brine ((a), (b)) and in LAPB+AOS surfactant ((c), (d)) before ((a), (c)) and after pressurization ((b), (d)) under temperature conditions (20 ºC).

3.2. Viscosity Measurement

The generated foam was injected into a capillary tube (L=0.83 m; D=0.000025 m) for viscosity measurements, and the pressure drop across the tube was recorded using pressure transducers. Foam apparent viscosity describes gas mobility reduction during foam flow, and depends strongly on the gas fraction f_g (foam quality, equation (1)) and foam texture in porous media (Rognmo et al., 2017). Foam apparent viscosity at f_g is calculated using equation (2) (Eftekhari and Farajzadeh, 2017). The foam quality, f_g, at which the maximum foam apparent viscosity occurs varies with NP and surfactant concentration (Eftekhari and Farajzadeh, 2017; Rognmo et al., 2017).

$$f_g = \frac{q_g}{q_g+q_s}, \quad (1)$$

$$\mu_{foam} = \frac{kA\Delta P}{(q_g+q_s)L}, \quad (2)$$

where A is the cross-sectional area of the tube, q_g and q_s are injection rates of gas and liquid, k is the absolute permeability, ΔP is the pressure drop across the tube with length L. The apparent foam viscosity at a gas fraction of f_g=0.70 was calculated to be μ_{foam} =11.44 cP.

3.3. Gas and foam injection

The images of the displacement experiments provide an effective method to track CO_2 plume and foam movement over time and to qualitatively detect distinctive displacement patterns (Fig. 6 and Fig. 8).

3.3.1. Gas injection

Fig. 6 shows images of gas displacement in the microfluidic device where brine is displaced by gas from left side to right side of the device. Under the injection rate of 0.1 μL/min, viscous fingers formed and significant amounts of brine were bypassed as a result. Higher injection rates (1 μL/min and 10 μL/min) appeared to lessen the viscous fingering effects. CO_2 saturation in the medium was quantified by analyzing pixel intensities in displacement images. CO_2 saturation as a function of injection time is shown in Fig. 7. Ultimate CO_2 saturation values of approximately 54%, 61%, 64 % were reached at volumetric injection rates of 0.1 μL/min, 1 μL/min and 10 μL/min, respectively. Gas fingers appeared along the displacement front in the medium due to hydrodynamic instability and unfavorable viscosity contrasts. This interfacial instability is undesirable in geological CO_2 sequestration processes (Rabbani et al., 2018).

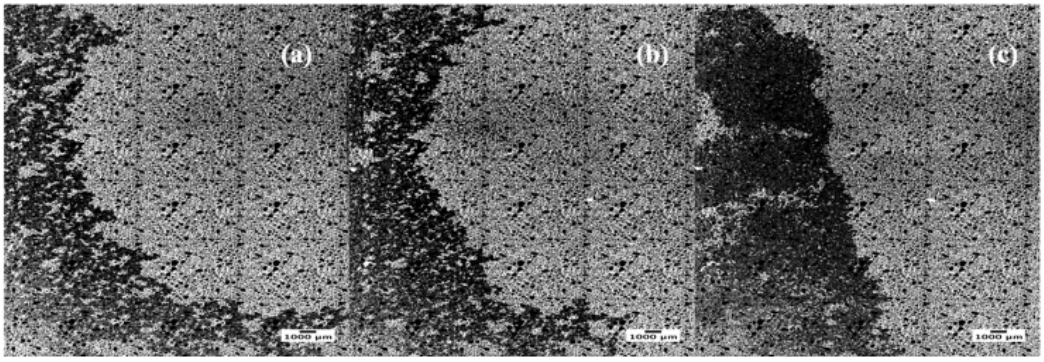

Fig. 6. The images of displacement fronts of gas injection at: (a) 0.1 μL/min, (b) 1 μL/min and (c) 10 μL/min (black areas are continuous foam phase).

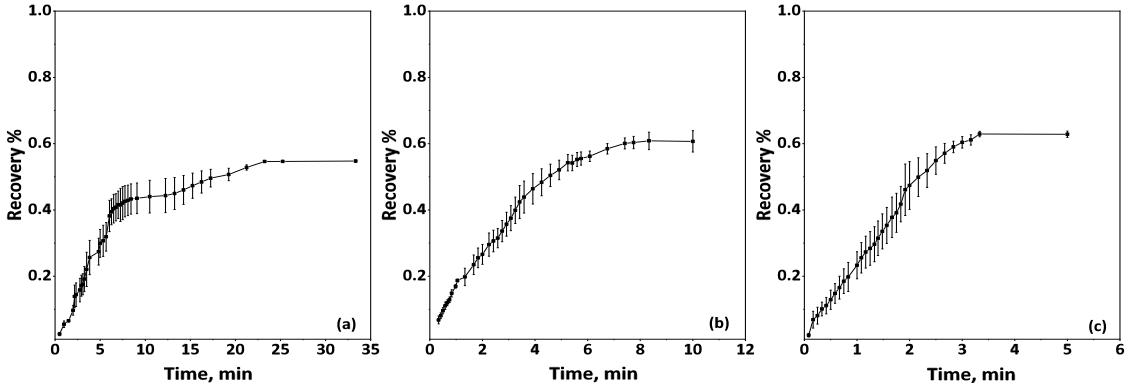

Fig. 7. The percentage of brine recovery from gas injection at: (a) 0.1 μL/min, (b) 1 μL/min and (c) 10 μL/min

3.3.2. Foam injection

Foam with a quality of f_g=0.70 was injected at three injection rates of 0.1 μL/min, 1 μL/min and 10 μL/min. High-resolution images were taken and analyzed to observe foam flow behavior and CO_2 saturation in the microfluidic device, shown in Fig. 8. The displacement interfaces between foam and brine appeared uniform and stable (no viscous fingering was observed). NP-stabilized

foams were highly stable and their relatively high apparent viscosity and lower mobility led to a higher ultimate CO_2 saturation in the medium compared to the case of gas injection (Guo and Aryana, 2016; Guo and Aryana, 2018; Guo et al., 2017). During the injection experiments, a continuous foam phase was observed invading the porous medium. The response due to the use of foam is dependent on the gas fraction (gas volume over the total volume of the foam) (Rognmo et al., 2017), making the generation of stable foams with high gas fractions critically important to storage process. CO_2 saturation values during foam injection experiments are shown in Fig. 9. Using an injection rate of 0.1 μL/min, the ultimate CO_2 saturation reached approximately 87%. Compared to gas injection, significant increases in the ultimate CO_2 saturation were observed in foam injection experiments; ultimate CO_2 saturation values increased by 33%, 34% and 35% at injection rates of 0.1 μL/min, 1 μL/min, and 10 μL/min, respectively. Therefore, nanoparticle-stabilized CO_2-water foam with high foam quality has the potential to increase CO_2 storage capacity compared to gaseous CO_2 injection (Afzali et al., 2018; Harper, 2012).

Introducing NP-stabilized CO_2 foam into an aquifer may also mitigate the risk of leakage of the stored CO_2 (Pizzocolo et al., 2017). A rapid pressure release from the outlet was conducted after five days of foam injection and CO_2 foam was regenerated when CO_2 and the NP-surfactant fluids flowed through the microfluidic device. To conclude, there are several potential advantages in injecting NP-stabilized CO_2 foam. The surfactant solution in the foam may mix with the resident brine (Worthen et al., 2014). After CO_2 foam is destabilized, the NP-surfactant solution would remain in the pore space, and if there is sudden fracture formation in the sealing layer above, CO_2 foam may be regenerated due to the resulting mixing of CO_2 and NP mixtures as they flow through the medium, which may help reduce the risk of CO_2 leakage (Irfan et al., 2018; Zheng et al., 2017).

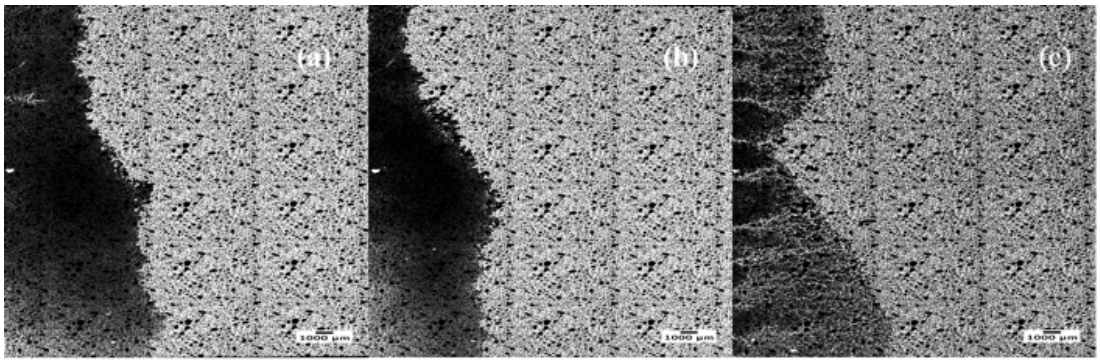

Fig. 8. The images of displacement fronts of foam injection at: (a) 0.1 μL/min, (b) 1 μL/min and (c) 10 μL/min (black areas are continuous foam phase).

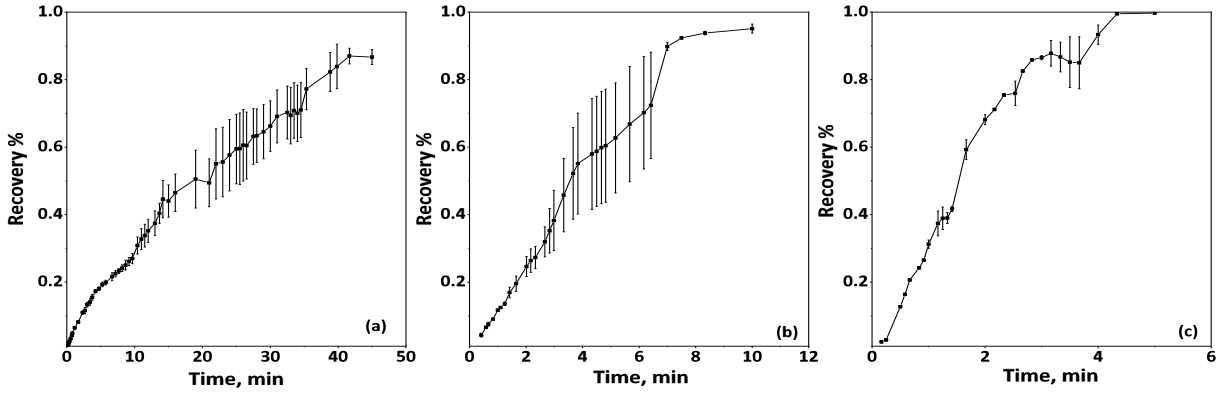

Fig. 9. The percentage of brine recovery from foam injection at: (a) 0.1 μL/min, (b) 1 μL/min and (c) 10 μL/min.

4. Conclusions

A series of injection experiments were conducted to study geological CO_2 sequestration in a saline aquifer by injecting gaseous, and NP-LAPB+AOS stabilized CO_2 foam into a microfluidic device. The contact angle and interfacial tension of CO_2 on Borofloat glass surrounded by brine and NP-LAPB+AOS solution were measured at the temperature and pressure conditions used in flow experiments. Flow experiment using a microfluidic device provided real-time visualization of CO_2 flow behaviour in a porous medium in the presence of brine. The observed flow regimes of the injected CO_2 and CO_2 foam were investigated using the corresponding capillary number and viscosity ratio values. The ultimate saturation of CO_2, i.e., CO_2 storage capacity, exhibits significant improvements in foam injection experiments compared to CO_2 injection experiments. In all foam flow experiments, the ultimate CO_2 saturation values increased by over 30% compared to the CO_2 injection cases. Results suggest that injection of a high-quality (f_g=0.70 in this case) CO_2 foam has the potential to significantly improve CO_2 storage capacity in an aquifer. The high foam stability resulting from the use of NPs as a stabilizer is critical to maintaining a high foam quality, prohibiting leakage and providing a safe geological CO_2 storage.

Acknowledgements

This material is based upon work supported by the U.S. Department of Energy National Energy Technology Laboratory Office of Fossil Energy under award number DE-FE0029465.

References

45Q, U.S.C., 2018. Credit for carbon oxide sequestration, in: U.S.C. (Ed.), 26

Adebayo, A.R., Kamal, M.S., Barri, A.A., 2017. An experimental study of gas sequestration efficiency using water alternating gas and surfactant alternating gas methods. Journal of Natural Gas Science and Engineering 42, 23-30.

Afzali, S., Rezaei, N., Zendehboudi, S.J.F., 2018. A comprehensive review on enhanced oil recovery by water alternating gas (WAG) injection. Fuel 227, 218-246.

Al-Khdheeawi, E.A., Vialle, S., Barifcani, A., Sarmadivaleh, M., Iglauer, S., 2017. Influence of CO2-wettability on CO2 migration and trapping capacity in deep saline aquifers. Greenhouse Gases: Science and Technology 7, 328-338.

Al-Menhali, A.S., Krevor, S., 2016. Capillary trapping of CO2 in oil reservoirs: Observations in a mixed-wet carbonate rock. Environmental science & technology 50, 2727-2734.
Aminzadeh, B., Chung, D.H., Bryant, S.L., Huh, C., DiCarlo, D.A., 2013. CO2 Leakage prevention by introducing engineered nanoparticles to the in-situ brine. Energy Procedia 37, 5290-5297.
Amirian, E., Dejam, M., Chen, Z., 2018. Performance forecasting for polymer flooding in heavy oil reservoirs. Fuel 216, 83-100.
Aryana, S.A., Kovscek, A.R., 2012. Experiments and analysis of drainage displacement processes relevant to carbon dioxide injection. Physical Review E 86, 066310.
Bachu, S., 2015. Review of CO2 storage efficiency in deep saline aquifers. International Journal of Greenhouse Gas Control 40, 188-202.
Barnes, J., Regalado, D.P., Doll, M., King, T., Pretzer, L., Semple, T., 2016. Essentials of upscaling surfactants for EOR field projects, SPE Improved Oil Recovery Conference. Society of Petroleum Engineers, Tulsa, Oklahoma, USA.
California Air Resources Board, 2018. Carbon capture and sequestration protocol under the low carbon fuel standard.
Carroll, K.C., McDonald, K., Marble, J., Russo, A.E., Brusseau, M.L., 2015. The impact of transitions between two-fluid and three-fluid phases on fluid configuration and fluid-fluid interfacial area in porous media. Water Resources Research 51, 7189-7201.
Chalbaud, C., Robin, M., Lombard, J.-M., Bertin, H., Egermann, P., 2010. Brine/CO2 interfacial properties and effects on CO2 storage in deep saline aquifers. Oil & Gas Science and Technology–Revue de l'Institut Français du Pétrole 65, 541-555.
Clark, J.A., Santiso, E.E., 2018. Carbon sequestration through CO2 foam-enhanced Oil recovery: a green chemistry perspective. Engineering, 4, 336-342.
Cui, L., Bourrel, M., 2018. Selection of CO2-soluble surfactants for CO2 foam/emulsion in hot and salty carbonate reservoirs, RDPETRO 2018: Research and Development Petroleum Conference and Exhibition, Abu Dhabi, UAE.
D. Riestenberg, 2018. Project ECO2S: Characterization of a world class carbon dioxide storage complex, Southern States Energy Board.
Dejam, M., Hassanzadeh, H., 2018. Diffusive leakage of brine from aquifers during CO2 geological storage. Advances in Water Resources, 111, 36-57.
Dixon, T., Leamon, G., Zakkour, P., Warren, L., 2013. CCS projects as Kyoto Protocol CDM activities. Energy Procedia 37, 7596-7604.
Eftekhari, A.A., Farajzadeh, R., 2017. Effect of foam on liquid phase mobility in porous media. Scientific Reports 7, 43870.
Ehtesabi, H., Ahadian, M.M., Taghikhani, V., Ghazanfari, M.H., 2014. Enhanced heavy oil recovery in sandstone cores using TiO2 nanofluids. Energy & Fuels 28, 423-430.
EPA, 2011. PSD and Title V permitting guidance for greenhouse gases. Air Quality Policy Division, Research Triangle Park, NC, USA.
EPA, 2018a. Inventory of U.S. greenhouse gas emissions and sinks: 1990-2016. US Environmental Protection Agency.
EPA, 2018b. Review of standards of performance for greenhouse gas emissions from new, modified, and reconstructed stationary sources: electric utility generating units.
Espinoza, D.N., Santamarina, J.C., 2010. Water-CO2-mineral systems: Interfacial tension, contact angle, and diffusion—Implications to CO2 geological storage. Water Resources Research 46.

Fu, T., 2016. Microfluidics in CO2 capture, sequestration, and applications, Advances in Microfluidics-New Applications in Biology, Energy, and Materials Sciences. InTechOpen.
Gershenzon, N.I., Ritzi, R.W., Dominic, D.F., Mehnert, E., 2017. Effective constitutive relations for simulating CO2 capillary trapping in heterogeneous reservoirs with fluvial sedimentary architecture. Geomechanics and Geophysics for Geo-Energy and Geo-Resources 3, 265-279.
Guo, F., Aryana, S.A., 2016. An experimental investigation of nanoparticle-stabilized CO2 foam used in enhanced oil recovery. Fuel 186, 430-442.
Guo, F., Aryana, S.A., 2018. Improved sweep efficiency due to foam flooding in a heterogeneous microfluidic device. Journal of Petroleum Science and Engineering 164, 155-163.
Guo, F., He, J., Johnson, P.A., Aryana, S.A., 2017. Stabilization of CO 2 foam using by-product fly ash and recyclable iron oxide nanoparticles to improve carbon utilization in EOR processes. Sustainable Energy & Fuels 1, 814-822.
Harper, E.J., 2012. Optimization of capillary trapping of CO2 sequestration in saline aquifers, Corvallis, Oregon: Oregon State University.
Hendraningrat, L., Torsæter, O., 2015a. Metal oxide-based nanoparticles: revealing their potential to enhance oil recovery in different wettability systems. Applied Nanoscience 5, 181-199.
Hendraningrat, L., Torsæter, O., 2015b. A study of water chemistry extends the benefits of using silica-based nanoparticles on enhanced oil recovery. Applied Nanoscience 6, 83-95.
Hosseini, H., Tsau, J., Peltier, E., Barati, R., 2018. Lowering fresh water usage in hydraulic fracturing by stabilizing scCO2 foam with polyelectrolyte complex nanoparticles prepared in high salinity produced water, SPE International Conference and Exhibition on Formation Damage Control. Society of Petroleum Engineers, Lafayette, Louisiana, USA.
IEA, 2019. Carbon capture, utilisation and storage, A critical tool in the climate energy toolbox, Paris Cedex 15 France.
Iglauer, S., 2017. CO2–Water–Rock wettability: variability, influencing factors, and implications for CO2 geostorage. Accounts of Chemical Research 50, 1134-1142.
IPCC, 2015. Climate change 2014: Mitigation of climate change, in: Change, I.P.o.C. (Ed.). Cambridge University Press, New York, NY, USA.
IPCC, 2018. Summary for policymakers of IPCC special report on global warming of 1.5°C approved by governments. The Intergovernmental Panel on Climate Change, New York, NY, USA.
Irfan, M.F., Bisson, T.M., Bobicki, E., Arguelles-Vivas, F., Xu, Z., Liu, Q., Babadagli, T., 2018. CO2 storage in saline aquifers by dissolution and residual trapping under supercritical conditions: An experimental investigation. Colloids and Surfaces A: Physicochemical and Engineering Aspects 548, 37-45.
Kamal, M.S., Adebayo, A.R., Fogang, L.T., Barri, A.A., 2018. Improving gas sequestration by surfactant-alternating-gas injection: a comparative evaluation of the surfactant type and concentration. Journal of Surfactants and Detergents 21, 667-675.
Kaveh, N.S., Rudolph, E.S.J., Wolf, K.-H.A., Ashrafizadeh, S.N.J.J.o.c., science, i., 2011. Wettability determination by contact angle measurements: hvbB coal–water system with

injection of synthetic flue gas and CO2. Journal of colloid and interface science 364, 237-247.
Krevor, S., Blunt, M.J., Benson, S.M., Pentland, C.H., Reynolds, C., Al-Menhali, A., Niu, B., 2015. Capillary trapping for geologic carbon dioxide storage – From pore scale physics to field scale implications. International Journal of Greenhouse Gas Control 40, 221-237.
Lenormand, R., Touboul, E., Zarcone, C., 1988. Numerical models and experiments on immiscible displacements in porous media. Journal of Fluid Mechanics 189, 165-187.
Lenormand, R., Zarcone, C., Sarr, A., 1983. Mechanisms of the displacement of one fluid by another in a network of capillary ducts. Journal of Fluid Mechanics 135, 337-353.
Leung, D.Y.C., Caramanna, G., Maroto-Valer, M.M., 2014. An overview of current status of carbon dioxide capture and storage technologies. Renewable and Sustainable Energy Reviews 39, 426-443.
Li, Y., Ranjith, P., Perera, M., Yu, Q., 2017. Residual water formation during the CO2 storage process in deep saline aquifers and factors influencing it: A review. Journal of CO2 Utilization 20, 253-262.
Michael, K., Golab, A., Shulakova, V., Ennis-King, J., Allinson, G., Sharma, S., Aiken, T., 2010. Geological storage of CO 2 in saline aquifers—a review of the experience from existing storage operations. International Journal of Greenhouse Gas Control 4, 659-667.
NASA, 2018. Long-term warming trend continued in 2017: NASA, NOAA, in: NASA (Ed.). NASA News & Feature Releases.
Office of Fossil Energy, 2019. Carbon storage research, Washington, DC, USA.
Otsu, N., 1979. A threshold selection method from gray-level histograms. IEEE Transactions on Systems, Man, and Cybernetics 9, 62-66.
Pal, N.R., Pal, S.K.J.P.r., 1993. A review on image segmentation techniques. Pattern Recognition 26, 1277-1294.
Pini, R., Krevor, S., 2019. Chapter 7 - Laboratory studies to understand the controls on flow and transport for CO2 storage, in: Newell, P., Ilgen, A.G. (Eds.), Science of Carbon Storage in Deep Saline Formations. Elsevier, pp. 145-180.
Pizzocolo, F., Peters, E., Loeve, D., Hewson, C.W., Wasch, L., Brunner, L.J., 2017. Feasibility of novel techniques to mitigate or remedy CO2 leakage, SPE Europec featured at 79th EAGE Conference and Exhibition. Society of Petroleum Engineers, Paris, France.
Rabbani, H.S., Or, D., Liu, Y., Lai, C.-Y., Lu, N.B., Datta, S.S., Stone, H.A., Shokri, N., 2018. Suppressing viscous fingering in structured porous media. PNAS 115, 4833-4838.
Rahman, A., 2018. Multiphase flow behavior during CO2 geo-sequestration in carbonate formations, in: Saghir, Z. (Ed.), ICTEA: International Conference on Thermal Engineering. ICTEA: International Conference on Thermal Engineering, Doha, Qatar.
Rathnaweera, T.D., Ranjith, P.G., Perera, M.S.A., 2015. Effect of salinity on effective CO2 permeability in reservoir rock determined by pressure transient methods: an experimental study on Hawkesbury sandstone. Rock Mechanics and Rock Engineering 48, 2093-2110.
Rognmo, A.U., Horjen, H., Fernø, M.A., 2017. Nanotechnology for improved CO2 utilization in CCS: Laboratory study of CO2-foam flow and silica nanoparticle retention in porous media. International Journal of Greenhouse Gas Control 64, 113-118.
Siddiqui, M.A.Q., Gajbhiye, R.N., 2017. Stability and texture of CO2/N2 foam in sandstone. Colloids and Surfaces A: Physicochemical and Engineering Aspects 534, 26-37.
Silverman, B.W., 2018. Density Estimation for Statistics and Data Analysis. Routledge.

Singh, H., Islam, A., 2018. Enhanced safety of geologic CO 2 storage with nanoparticles. International Journal of Heat and Mass Transfer 121, 463-476.
Stjernström, M., Roeraade, J., 1998. Method for fabrication of microfluidic systems in glass. Journal of Micromechanics and Microengineering 8, 33-38.
Szeliski, R., 2010. Computer vision: algorithms and applications. Springer Science & Business Media.
USGCRP, 2018. Fourth national climate assessment, in: Program, U.S.G.C.R. (Ed.), Washington, DC, USA.
Vitoonkijvanich, S., AlSofi, A.M., Blunt, M.J., 2015. Design of foam-assisted carbon dioxide storage in a North Sea aquifer using streamline-based simulation. International Journal of Greenhouse Gas Control 33, 113-121.
Wang, Y., Aryana, S.A., 2019. Creation of saturation maps from two-phase flow experiments in microfluidic devices, in: Banerjee, S., Barati, R., Patil, S. (eds.), Advances in Petroleum Engineering and Petroleum Geochemistry. Advances in Science, Technology & Innovation (IEREK Interdisciplinary Series for Sustainable Development). Springer, Cham.
Worthen, A.J., Parikh, P.S., Chen, Y., Bryant, S.L., Huh, C., Johnston, K.P.J.E.P., 2014. Carbon dioxide-in-water foams stabilized with a mixture of nanoparticles and surfactant for CO2 storage and utilization applications. Energy Procedia 63, 7929-7938.
Xu, K., Zhu, P., Huh, C., Balhoff, M.T., 2015. Microfluidic investigation of nanoparticles' role in mobilizing trapped oil droplets in porous media. Langmuir 31, 13673-13679.
Yang, D., Wang, S., Zhang, Y., 2014. Analysis of CO2 migration during nanofluid-based supercritical CO2 geological storage in saline aquifers. Aerosol Air Quality Research 14, 1411-1417.
Yang, W., Peng, B., Liu, Q., Wang, S., Dong, Y., Lai, Y., 2017. Evaluation of CO2 enhanced oil recovery and CO2 storage potential in oil reservoirs of Bohai Bay Basin, China. International Journal of Greenhouse Gas Control 65, 86-98.
Zhang, C., Oostrom, M., Wietsma, T.W., Grate, J.W., Warner, M.G., 2011. Influence of viscous and capillary forces on immiscible fluid displacement: Pore-scale experimental study in a water-wet micromodel demonstrating viscous and capillary fingering. Energy & Fuels 25, 3493-3505.
Zhao, B., MacMinn, C.W., Juanes, R., 2014. Residual trapping, solubility trapping and capillary pinning complement each other to limit CO2 migration in deep saline aquifers. Energy Procedia 63, 3833-3839.
Zheng, X., Mahabadi, N., Yun, T.S., Jang, J., 2017. Effect of capillary and viscous force on CO2 saturation and invasion pattern in the microfluidic chip. Journal of Geophysical Research: Solid Earth 122, 1634-1647.